Sheath structure transition controlled by secondary electron emission

2015 Plasma Sources Sci. Technol. 24 025012

(http://iopscience.iop.org/0963-0252/24/2/025012)

IOP Publishing Plasma Sources Science and Technology

Plasma Sources Sci. Technol. **24** (2015) 025012 (9pp) doi:10.1088/0963-0252/24/2/025012

Sheath structure transition controlled by secondary electron emission

I V Schweigert[1,2,3], S J Langendorf[4], M L R Walker[4] and M Keidar[1]

[1] George Washington University, Washington, DC 20052, USA
[2] Khristianovich Institute of Theoretical and Applied Mechanics, Novosibirsk 630090, Russia
[3] Novosibirsk State University, Novosibirsk 630090, Russia
[4] Georgia Institute of Technology, Atlanta, GA 30332, USA

E-mail: ivschweigert@email.gwu.edu

Received 24 November 2014, revised 27 December 2014
Accepted for publication 13 January 2015
Published 13 February 2015

Abstract

In particle-in-cell Monte Carlo collision (PIC MCC) simulations and in an experiment we study sheath formation over an emissive floating Al_2O_3 plate in a direct current discharge plasma at argon gas pressure 10^{-4} Torr. The discharge glow is maintained by the beam electrons emitted from a negatively biased hot cathode. We observe three types of sheaths near the floating emissive plate and the transition between them is driven by changing the negative bias. The Debye sheath appears at lower voltages, when secondary electron emission is negligible. With increasing applied voltage, secondary electron emission switches on and a first transition to a new sheath type, beam electron emission (BEE), takes place. For the first time we find this specific regime of sheath operation near the floating emissive surface. In this regime, the potential drop over the plate sheath is about four times larger than the temperature of plasma electrons. The virtual cathode appears near the emissive plate and its modification helps to maintain the BEE regime within some voltage range. Further increase of the applied voltage U initiates the second smooth transition to the plasma electron emission sheath regime and the ratio $\Delta\phi_s/T_e$ tends to unity with increasing U. The oscillatory behavior of the emissive sheath is analyzed in PIC MCC simulations. A plasmoid of slow electrons is formed near the plate and transported to the bulk plasma periodically with a frequency of about 25 kHz.

Keywords: discharge plasma, emissive wall, boundary sheath effect

1. Introduction

The plasma–wall interaction is the fundamental process determining plasma properties in laboratory plasmas. Materials with enhanced secondary electron emission (SEE) used for manufacturing electrodes and walls in discharge chambers change the classical concept of the Debye sheath, screening plasma from the surface [1–7]. Depending on the ratio of plasma and secondary electron temperatures, the sheath near the emissive wall rearranges itself [1, 2], which essentially affects the plasma parameters. For example, the effect of two types of wall materials with high and low SEEs was studied in the experiment [8] for the Hall thruster plasma. It was shown there that with applied voltage, the plasma electron temperature T_e increases linearly for the low-emission case, but plateaus for the case of an emissive surface, which changes all plasma characteristics.

The recent studies consider an interaction of an emissive wall with (i) a Maxwellian plasma and (ii) a non-Maxwellian plasma with a high energy beam. For Maxwellian plasma–wall interaction the classical theory of Hobbs and Wesson [1] indicates the potential drop of $\sim T_e$ over the emissive wall sheath and the existence of a space charge limited (SCL) regime for sheaths. The theory predicts that the SCL occurs at a wall electron yield close to unity. Further increase of wall emission creates a non-monotonic potential dip structure, repelling the additional electrons back to the wall surface. This is why the sheath is known as 'space charge limited', and the potential dip structure has been referred to as a virtual cathode. In 1988, Intrator *et al* [9] measured sheaths over a thermionically emitting grid using emissive probes. The results showed a profile similar to the Hobbs and Wesson prediction, with a virtual cathode. The authors questioned how such a structure could be stable, reasoning that slow ions would become trapped

in the potential dip and neutralize it. The conclusion was that ions were transported away out of the plane of the sheath, a process which was called ion pumping. In [7], the simulations and experiment in rf discharge afterglow demonstrated that for the case of a Maxwellian plasma–wall interaction the emissive sheath potential goes to zero as the plasma electron temperature approaches the emitted electron temperature.

A non-Maxwellian plasma–emissive wall interaction was studied in particle in cell (PIC) simulations [2–4, 9] and with kinetic analysis [10] for the Hall thruster plasma parameters. It was shown that the different sheath configurations may exist beyond the classical picture of the Hobbs and Wesson sheath if electron emission from the wall increases. The sheath potential profile over an electrically isolated surface may flatten and even drive the wall to a higher potential than the plasma. The plasma sheath can also be in a quasi-steady SCL state, performing the relaxation oscillations [2]. Recently Sheehan *et al* [11] observed a sheath with a virtual cathode over a dielectric-coated wall, but the sheath retained a large potential drop similar to that of a non-emitting wall. There is thus a need for additional experimental measurements and kinetic simulations of sheaths over emitting walls to clarify the sheath dynamics and structure.

In this work on two-dimensional (2D) kinetic simulations with the PIC Monte Carlo collision (MCC) method and in the experiment we study a non-Maxwellian plasma (with an electron beam) interaction with an emissive electrically isolated plate. Our goal is to identify the transition between different types of sheath near the emissive floating plate driven by an increase of electron beam energy. We consider a large-volume direct current (dc) discharge plasma to exclude complex effects occurring in the Hall thruster channel.

This paper is organized as follows. The experimental setup is described in section 2. The kinetic model for the 2D description of the dc discharge is given in section 3. The three types of sheaths and transition between them is described in section 4. The electron energy distribution functions for different sheath types are compared in section 5. The quasi-steady state of the sheath with oscillations is discussed in section 6. The conclusions are given in section 7.

2. Experimental setup

In the experiment, we use a multidipole plasma device with confining cusp fields from permanent magnets as shown in figure 1. The chamber has a cylindrical shape with radius $r = 30.5$ cm and height $h = 91$ cm. The aluminum walls of the chamber are grounded and have low SEE yield. The dc discharge glows in argon at the pressure $P = 10^{-4}$ Torr. The discharge plasma is sustained by an electron beam emitted by a hot cathode, which is a tungsten filament (denoted by F in figure 1). The voltage U applied to the cathode ranges from -60 to -120 V. The thermoemission electron current from the cathode j varies from 10 to 40 mA. The dielectric plate made from Al_2O_3 is placed 40 cm apart from the cathode. This plate is denoted by W in figure 1. The sheath structure is measured over the sheath near this plate, which is electrically isolated and has enhanced secondary emission yield.

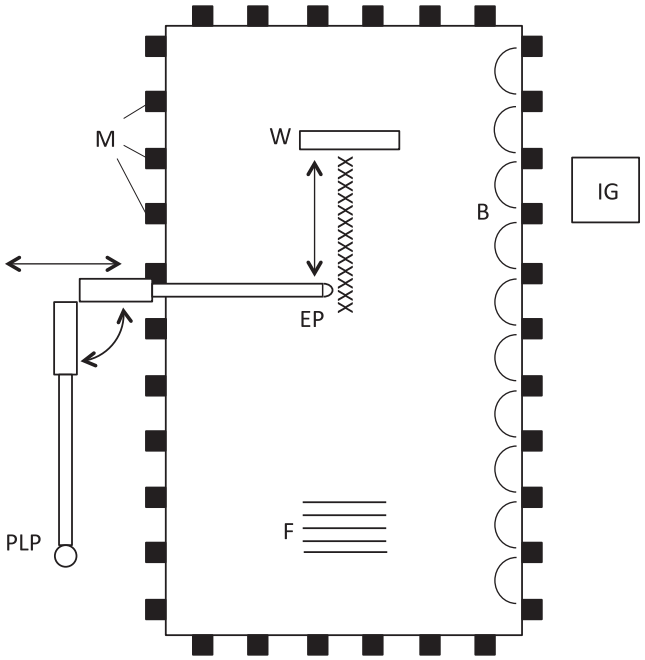

Figure 1. Schematic of experimental layout. Cathode (F), magnets (M), nominal magnetic field (B), planar Langmuir probe (PLP), emissive probe (EP), and emissive floating plate made from Al_2O_3 (W). Emissive probe orientation rotated 90° to show hairpin tip geometry.

Plasma electron density and temperature are measured with a planar Langmuir probe. The sheath potential profiles are measured with a swept emissive probe. It is constructed of telescoping alumina tubing and a hairpin 0.005 inch diameter thoriated tungsten filament emissive tip. The planar probe data is found to fit well to the equation for the probe current from the primary electrons given by Hershkowitz [14], and from the remaining bi-Maxwellian plasma by the analysis of Knapmiller *et al* [15], correcting for the SEE of the tungsten probe tip using the data of Hagstrum [16].

Our device is similar to the original design by Limpaecher and Mackenzie [12] used in the work of Hershkowitz [13]. Different from previous work, we operate the device at a low discharge current of 10–40 mA in order to allow the energetic electrons from the cathode to become a significant population in the plasma. This increases the average electron energy of the plasma and elicits high SEE yields from the wall materials. Rather than the enclosed-type multidipole device in which the device itself is the vacuum vessel, the present device is constructed of a series of aluminum rails placed within a larger vacuum chamber. Neutral molecules enter the device from the vacuum chamber, which receives mass flow input directed away from the device to allow the gas to expand throughout the chamber and enter the device with a spatially uniform number density.

3. Kinetic model and calculation details

3.1. Model setup

In our simulations, the discharge chamber is smaller than in the experiment, $r = 20$ cm and $h = 50$ cm. The calculation

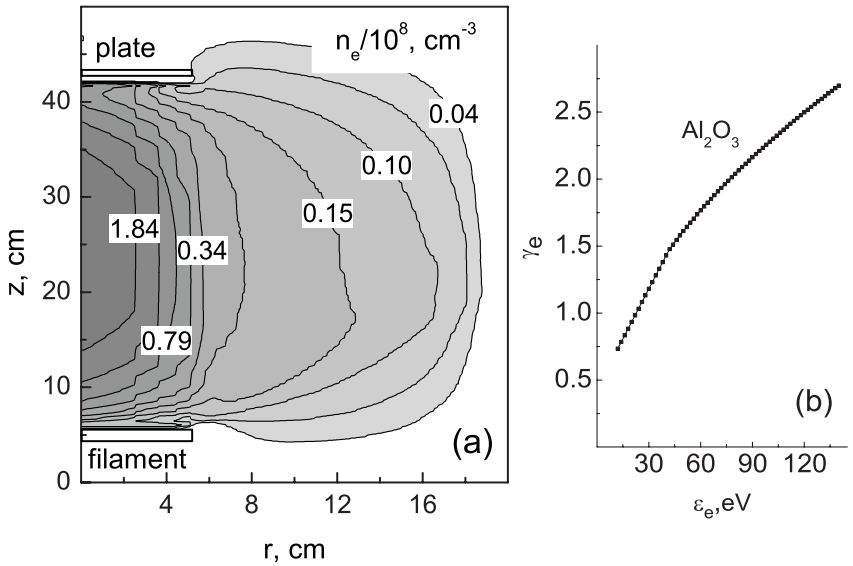

Figure 2. (*a*) Electron density normalized with $10^8\,\mathrm{cm}^{-3}$ for thermoemission current $j = 30\,\mathrm{mA}$ and the applied voltage $U = -70\,\mathrm{V}$. The axis of symmetry of the cylindrical chamber is at $r = 0$. (*b*) SEE coefficient as a function of the electron energy for Al_2O_3 material.

cell of the cylindrical chamber is shown in figure 2. The cathode is at $z = 5.6\,\mathrm{cm}$, and the plate is placed some distance, $d = 36.4\,\mathrm{cm}$, away from the cathode. Both the cathode and the plate are disks with radii of 5 cm.

In our kinetic study we use a simplified model of the experimental setup, which does not include a magnetic field. This assumption should not change the qualitative picture of the transition, since the magnetic field is non-zero only near the wall of the chamber and does not affect the beam electron motion. In the experiment, the cathode is situated in front of the floating emissive plate. The electrons starting from the hot cathode due to the thermoemission gain large kinetic energy crossing the potential drop over the cathode sheath. These electrons have longitudinal components of velocity $v_z \gg v_x, v_y$ and form a beam which is directed to the emissive plate surface. Another group of electrons (plasma electrons) has a low mean energy and is trapped inside of the chamber by the wall sheath potential drop even without a magnetic field. The presence of a magnetic field near the wall reduces the losses of the higher energy part of the plasma electrons and increases the ionization rate. This is why the density of plasma in experiment is higher than that in simulations. This difference can shift the critical point of transition between different sheaths.

3.2. System of equations

In our model, the plasma is described by the system of equations which includes the kinetic equations for electrons and ions, Poisson's equation for electrical potential and the current balance equation for the plate floating potential. Our model is two-dimensional with cylindrical symmetry and electron and ion energy distribution functions (EEDFs and IEDFs) that are three-dimensional in terms of velocity and two-dimensional in space (known as 2D3V). The energy distribution function for electrons $f_e(\vec{r}, \vec{v})$ and ions $f_i(\vec{r}, \vec{v})$ are found from the Boltzmann equations

$$\frac{\partial f_e}{\partial t} + \vec{v}_e \frac{\partial f_e}{\partial \vec{r}} - \frac{e\vec{E}}{m}\frac{\partial f_e}{\partial \vec{v}_e} = J_e, \quad n_e = \int f_e \, \mathrm{d}\vec{v}_e, \tag{1}$$

$$\frac{\partial f_i}{\partial t} + \vec{v}_i \frac{\partial f_i}{\partial \vec{r}} + \frac{e\vec{E}}{M}\frac{\partial f_i}{\partial \vec{v}_i} = J_i, \quad n_i = \int f_i \, \mathrm{d}\vec{v}_i, \tag{2}$$

where v_e, v_i, n_e, n_i, m and M are the electron and ion velocities, concentrations and masses, respectively; J_e and J_i are the collisional integrals for electrons and ions with background atoms. Knowing the energy distribution functions for electrons and ions, we can calculate the mean energy of ions and electrons.

Applying a zero-current balance equation to the surface of a floating emissive plate

$$j_{be} + j_{pe} + j_i + j_{es} + j_{esr} = 0, \tag{3}$$

where j_{be} is the current of beam electrons from plasma, j_{pe} is the current of plasma electrons, j_i is the ion current, j_{es} is the current of secondary electrons emitted from the plate surface and j_{esr} is the current of secondary electrons, returning back to the surface. Poisson's equation describes the electric potential distribution

$$\triangle \phi = 4\pi e \left(n_e - \sum_{i=1}^{N} n_i \right), \quad \vec{E} = -\frac{\partial \phi}{\partial \vec{r}}. \tag{4}$$

The boundary conditions for Poisson's equation are the voltage $U = 0$ on the grounded wall of the chamber and $U = U_0$ on the cathode. The floating potential of the emissive plate is calculated self-consistently from the condition of a zero total current onto the plate surface.

The discharge operates in argon. The kinetics of electrons includes elastic scattering of electrons on background atoms, excitation of metastable states, and ionization. The cross sections of electron scattering for argon are taken from [17, 18]. For Ar^+ ions, the elastic collision on background atoms with isotropic scattering and resonant charge exchange collision, or backward elastic scattering, are taken into account.

3.3. Model of SEE from the plate

In both model and experiment the plate is made from Al_2O_3. This material has a large secondary emission coefficient due to the electron bombardment γ_e, which increases with the energy of an incident electron [19]. The electron emission is calculated by accounting for the energy distribution functions of the beam and plasma electrons. Figure 2(*b*) shows the SEE coefficient as a function of the electron energy for Al_2O_3. In simulation we assume that there is no SEE for electrons with an energy of less than 10 eV. If $\epsilon_e \geqslant 10$ eV and $\gamma_e(\epsilon_e) < 1$, a random number (RN) is computed from uniformly distributed random numbers in the interval [0,1]. Then if RN $< \gamma_e(\epsilon_e)$, a secondary electron with the weight of an incident electron (w_e) is emitted from the surface. The term 'weight' denotes the number of electrons in a group with the same velocity and coordinate and varies depending on the plasma density, $w_e = (2 \div 4) \times 10^4$. If $\gamma_e(\epsilon_e) > 1$, a secondary electron with the weight $w_e \times \gamma_e(\epsilon_e)$ is emitted. In our simulations, the emitted electrons have a half-Maxwellian distribution with the temperature equal to 0.1 eV.

3.4. Simulation details

System (1)–(4) is solved self-consistently by the 2D3V PIC method with sampling of collisions by the Monte Carlo method (2D3V PIC MCC) [20, 21]. The 2D3V PIC MCC method is based on sampling of EEDF and IEDF by pseudoparticles (PPs). It has been shown [22] that in the limit of a small time step and large number of PPs the PIC MCC model converges to a solution of the Boltzmann's equation.

The simulation grid is uniform over z with $\Delta z = 0.1$ cm, that is less than the Debye length. The computational grid over axis r is thickened at the edge of the electrode. The minimum and maximum grid steps over r are 0.1 cm and 0.25 cm respectively. The time step is $\Delta t = 0.5 \times 10^{-12}$ s, that is much less than the Courant number ($\Delta z/v_e \simeq 10^{-10}$ s). In our case the plasma frequency $\omega_e \simeq 10^9$ s^{-1} and the electron scattering frequency $\nu_e \simeq 10^7$ s^{-1} give less restriction for the time step. The number of PPs for every type of species is $(2 \div 4) \times 10^6$ depending on the plasma conditions.

For definition of the floating potential ϕ_s of the emissive plate, during PIC MCC simulation the currents of electrons and ions into and from the emissive plate are periodically calculated. The total current (integrated for every 1 μs time interval) should be zero with an accuracy of 2%. If not, then the floating potential is adjusted with a small value of 0.1 V to improve the zero-current balance.

The calculations are performed with the 2D3V PlasmaNov code, which is a PIC MCC code developed by V A Schweigert in 1998 (see, for example, [23]). Previously the 2D3V PlasmaNov parallelized code was successfully applied for simulations of plasma discharges with the non-local-electron and ion distribution functions. For example, for modeling the effect of high-frequency capacitive (HFC) discharge and magnetic field on the plasma layer near the surface in hypersonic gas flow [24], for active control of EEDF in dc discharge [25], for control of ion flux formation in an asymmetric HFC discharge [26] and for studying transition modes in HFC discharge in methane [27].

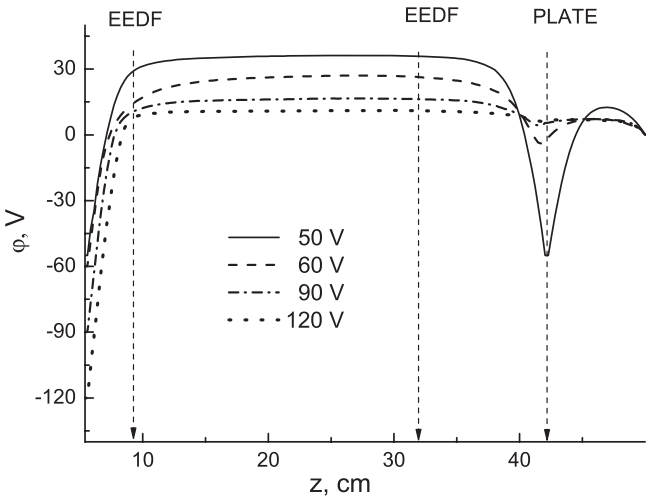

Figure 3. Potential profiles over axis of symmetry for the applied voltage of −55 V, −60 V, −90 V and −120 V and for thermoemission current $j = 20$ mA. The cathode is at $z = 5.6$ cm and the plate is at $z = 42$ cm. Vertical arrows show the place of calculation of the EEDF.

4. Three types of sheaths

For our experimental conditions the plasma density varies from 10^7 to 5×10^8 cm^{-3}. The calculated electron density n_e distribution shown in figure 2 has a maximum value in the central part of the chamber volume. The Debye sheath forms near the non-emissive walls and there the n_e is close to zero. The potential drop over the wall sheath confines the plasma electrons. In figure 3, the potential distribution over the axis of symmetry is shown for different voltages and $j = 20$ mA. The potential drop over the cathode sheath increases with the negative bias, whereas the plasma potential slightly decreases. The electrons emitted from the hot cathode cross the sheath practically without collisions and gain the kinetic energy proportional to the potential drop. These beam electrons provide the ionization rate $\nu_i \approx 10^{13}$ cm^{-3} s^{-1} in the discharge volume for our plasma parameters.

Both in the experiment and simulation we observe a non-monotonic decrease of the sheath over the floating emissive plate with the rise of the beam electron energy. This non-monotonic behavior of the plate potential drop $\Delta\phi_s$ is explained by changing the current balance into the plate. The measured and calculated potential distribution near the plate are shown in figures 4 and 5 for negative biases ranging from −60 to −120 V. The potential profiles are given relative to the plasma potential. The computed and measured values of potential drops coincide within 10% error. But the measured and computed sheaths near the plate differ in size by a factor of 2, because the density of plasma in simulation is smaller. A virtual cathode near the plate can be seen only on computed potential profiles in figures 4(*b*) and 5(*b*). This potential dip is created due to the excess of slow secondary electrons. No virtual cathode was observed in the experiments, which may be due to insufficient probe resolution near the wall.

A more detailed picture of the modification of the potential drop near the emissive plate $\Delta\phi_s$ and the virtual cathode dip $\Delta\phi_d$ is shown in figure 6. We observe three types of the sheaths

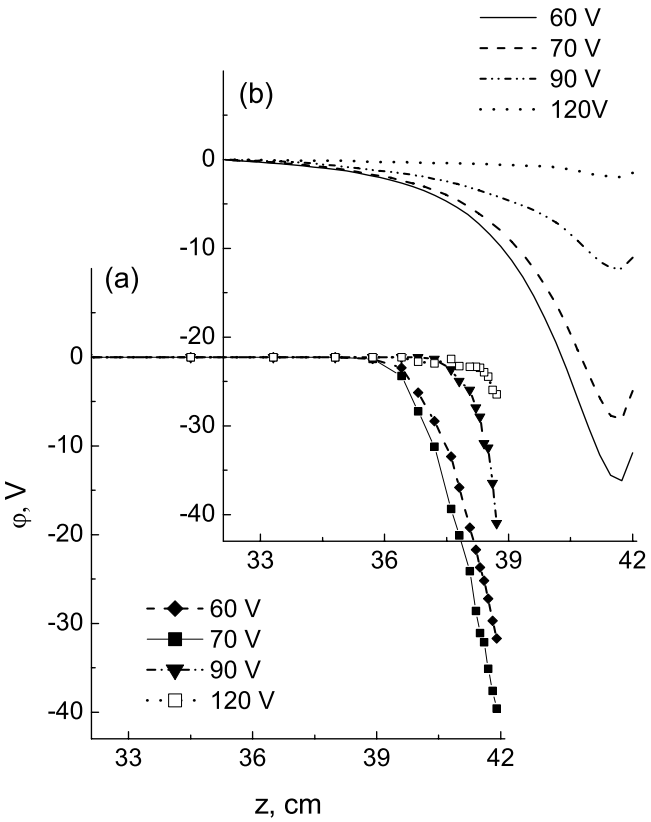

Figure 4. Measured (a) and calculated (b) potential distribution near the emissive plate for $U = -60, -70, -90$ and -120 V at $j = 10$ mA.

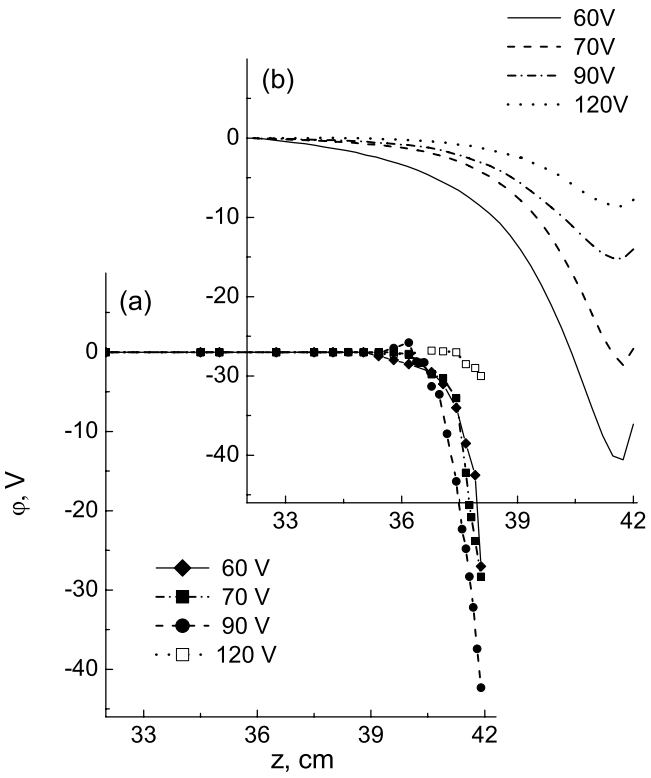

Figure 5. The same as in figure 4, but at $j = 40$ mA.

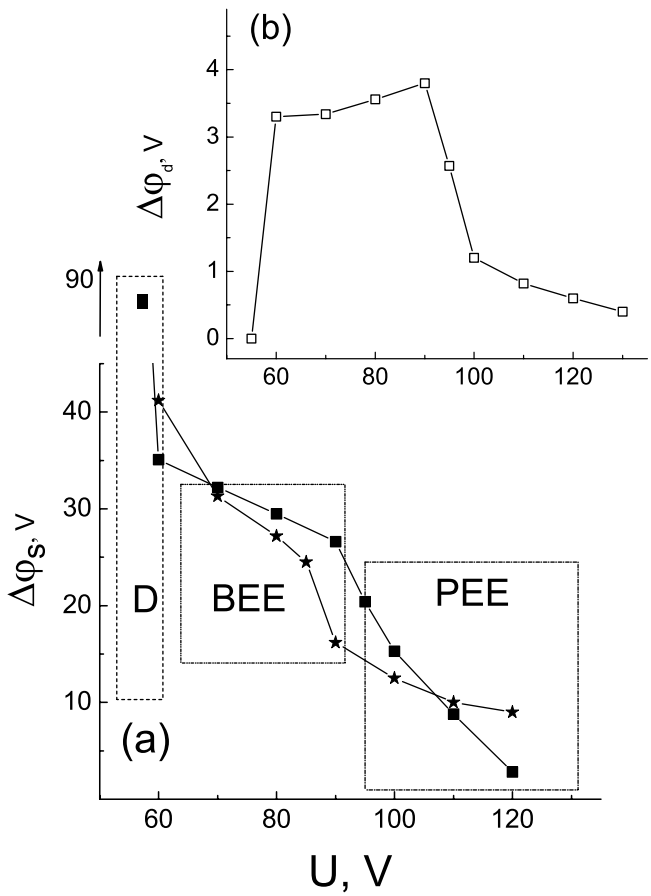

Figure 6. (a) Potential drop over the plate sheath $\Delta\phi_s$ relative to the plasma potential for $j = 20$ mA (squares) and $j = 40$ mA (stars), and (b) the virtual cathode dip $\Delta\phi_d$ relative to the plate surface for $j = 20$ mA. Debye sheath regime (D), electron beam emission (BEE) and plasma electron emission (PEE) regimes are shown.

over the plate, and the transition between them is driven by changing the negative bias U.

Debye sheath. First, at lower voltage $|U| < 60$ V, the classical Debye sheath similar to the cathode's and wall's sheaths occurs over the plate. It is indicated by a square D in figure 6(a). For this case, the potential drop near the emissive plate $\Delta\phi_s = 87$ V, which is about the cathode potential drop and a virtual cathode is absent (see figure 6(b)). Since the $\Delta\phi_s$ is large, the beam electrons, approaching the plate, have low energy and the SEE is negligible. The beam electron current j_{be} together with the ion current j_i provide the zero-current condition on the plate. The total electron and ion currents to the plate for different U and $j = 20$ and 40 mA are shown in figure 7. The ion current calculated with the semi-empirical Bohm's formula, $j_i = 0.4neS(2kT_e/m_i)^{0.5}$, agrees well with our PIC-calculated j_i.

BEE regime. With increasing U, the transition from the Debye sheath (D) regime to the BEE regime takes place at $|U| = 60$ V. This transition is induced by switching on the SEE and accompanied by a considerable rise of the electron current from the plasma to the plate. As seen in figure 7, after transition from the D regime to the BEE one, the electron current to the plate rises by two orders of magnitude. Now the beam electron flux from the plasma and the secondary electron

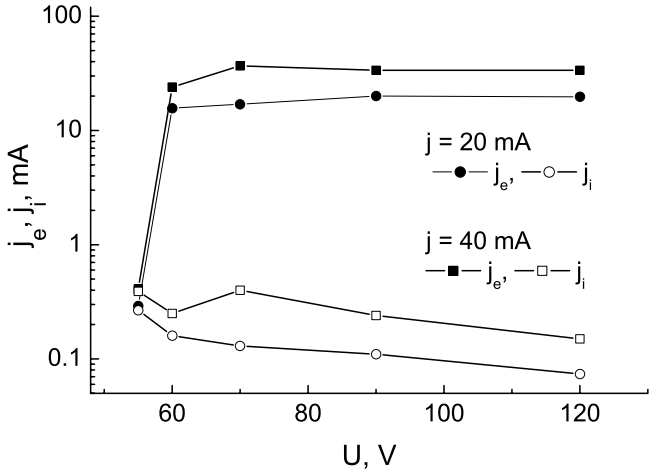

Figure 7. Total electron j_e and ion currents to the plate surface as a function of negative bias for $j = 20$ and 40 mA.

current j_{es} set the floating plate potential, $j_{be} = j_{es} - j_{esr}$, where j_{esr} is the secondary electrons, returning back to the surface by the virtual cathode.

Since the plate potential drop decreases after the transition, the beam electrons approach the plate with energy greater than 40 eV. In this case the SEE yield is $\gamma_e > 1$ and the virtual cathode appears just after the transition. With further increase of the electron beam energy (with increasing U) the potential dip of the virtual cathode becomes larger, returning more secondaries back to the surface. This increase of the potential dip helps the BEE regime to survive for some range of voltage.

The measured and calculated mean temperature of the plasma electrons T_e as a function of U is shown in figure 8. For all considered cases $T_e/T_{es} > 10$, since the mean temperature of secondaries is $T_{es} = 0.1$ eV. In the BEE regime, the potential drop over the plate sheath is essentially larger than the mean energy of plasma electrons, $\Delta\phi_s/T_e \approx 4 \div 5$.

PEE regime. The second transition is smooth and happens at $U \approx 90$ V for the discharge current ranging from 10 to 40 mA. It is clearly indicated in figure 6 by a faster decrease of the plate potential drop and shrinking of the virtual cathode. The mean temperature of the plasma electrons T_e also decreases at the point of the transition. In this new regime, the cold plasma electrons start to contribute to the zero-current balance on the plate. Let us call this regime a PEE regime. Now the currents of the cold plasma electrons j_{pe}, beam electrons j_{be} and secondary electrons, $j_{be} + j_{pe} = j_{se} + j_{ser}$ set the ϕ_s. The term j_{ser} becomes comparably small, because the virtual cathode practically disappeared (see figures 4(*b*) and 5(*b*)). Since the density of the slow plasma electrons is much larger than that of the beam electrons, a small decrease of $\Delta\phi_s$ leads to considerable increase of the plasma electron current. With increasing U the $\Delta\phi_s$ tends to $1T_e$.

5. Electron energy distribution function

The electrons emitted from the negatively biased hot cathode compose a beam of the same radius as the cathode. This beam

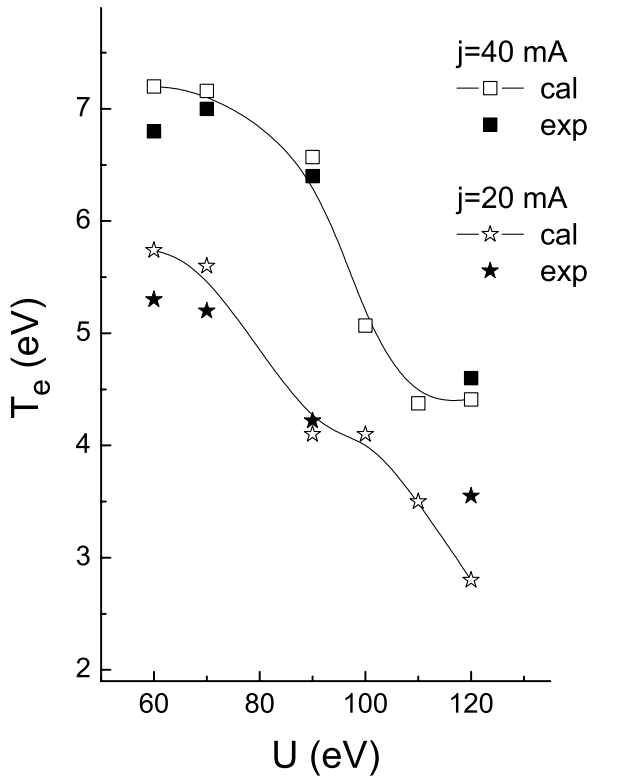

Figure 8. Mean electron temperature of plasma electrons in the center of discharge as a function of negative bias on the cathode for $j = 20$ mA (stars) and 40 mA (squares). The open symbols are from simulations and closed symbols are from experiment.

is directed to the emissive floating plate. The electron energy distribution functions shown in figure 9 were calculated on the axis of symmetry at the cathode sheath–plasma boundary and in bulk plasma. In figure 3, the vertical arrows show the points of the EEDF calculation. The plasma parameters determining the shape of the EEDF for $j = 20$ mA are listed in table 1. In figure 9, the EEDFs calculated at the sheath–plasma boundary (at $x = 9$ cm) and in bulk plasma (at $z = 32$ cm) exhibit peaks of beam electrons with energy of about 85 eV, which is equal to the cathode potential drop. The EEDF in bulk plasma has a peak with a wider distribution due to collisions with background atoms and the oscillative nature of the plate sheath. The groups of low energy electrons have a mean temperature of 6.5 eV. Since the potential drop near the plate is 35 V for $U = -70$ V (see table 1), the secondary electrons have sufficient energy for the ionization. These secondaries enrich the higher energy part of the plasma electron spectrum.

To explain the transition between the BEE and PEE sheath regimes in terms of EEDF, let us consider the spectrum of electrons arriving to the plate surface. In figure 10, the EEDF is shown for $j = 20$ mA and for different voltages. It is seen that already for $U = 60$ V, the energy of beam electrons approaching the plate surface is large enough (≈50 eV) to provide $\gamma_e > 1$. The large potential drop (35 V) screens the plate from the most plasma electrons, therefore their fraction in the EEDF is small (<0.1%) compared to that of the beam electrons. The energy distribution function of electrons arriving on the plate is a shifted EEDF at $z = 32$ cm, where a shift is the potential drop near the plate, $\Delta\phi_s$.

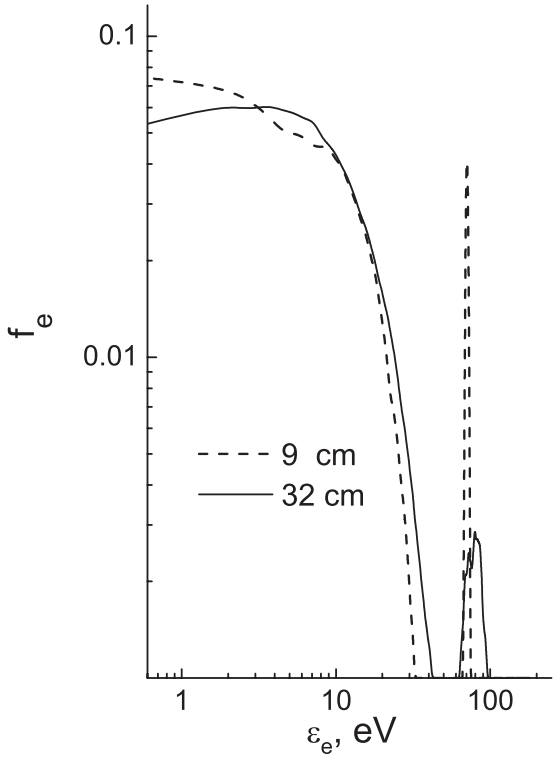

Figure 9. Electron distribution function over energy at $z = 9$ cm (dashed line), 32 cm (solid line) for $j = 20$ mA, $U = -70$ V.

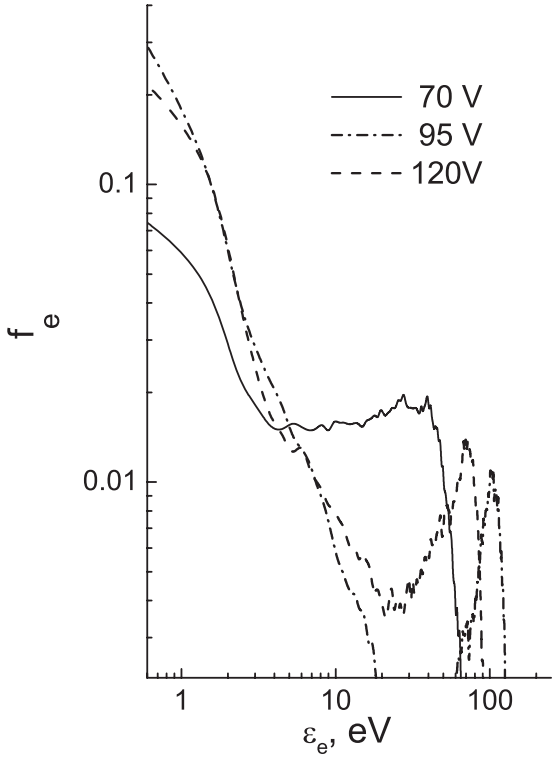

Figure 10. Energy distribution function for electrons approaching the plate surface for $U = -70$ V (solid line), -95 V (dashed line) and -120 V (dashed–dotted line) for $j = 20$ mA.

Table 1. Negative bias (U), beam electron energy (ϵ_{be}), plate sheath potential drop ($\Delta\phi_s$), mean temperature of plasma electrons (T_e), and virtual cathode potential dip ($\Delta\phi_d$) for $j = 20$ mA.

U (V)	70	95	120
ϵ_{be} (eV)	84	115	130
$\Delta\phi_s$ (V)	35.1	20.4	2.9
T_e (eV)	5.7	4.2	2.8
$\Delta\phi_d$ (eV)	3.3	2.56	0.57

With increasing voltage U, the shape of the EEDF changes qualitatively. The fraction of slow electrons from the plasma essentially increases as a result of the transition between the BEE and PEE regimes. At $U > 90$ V the beam electrons approaching the plate have an energy of around 100 eV. They produce so many secondaries that the plate sheath potential decreases, allowing the colder plasma electrons to reach the plate and support the zero-current balance. The virtual cathode becomes considerably smaller and fewer secondaries repel back to the plate. The electron current from the plasma to the plate is set both by plasma electrons and beam electrons, and the partial contribution of the plasma electron current increases to 0.55 for $U = 120$ V.

6. Sheath oscillations near the emissive plate

The formation of a virtual cathode near the emissive wall in a Maxwellian plasma was found previously in simulations [1] and observed in the experiment [9]. In our case, the virtual cathode appears after the transition from the Debye sheath regime to the BEE one. It is known that the virtual cathode appears when the total electron flux from the plasma produces a larger flux of secondaries. In figure 11, the electron and ion density profiles over the plate are shown for the Debye ($U = -55$ V) and BEE ($U = -60$ V) sheathes. In the Debye sheath, as expected, $n_i \gg n_e$. The BEE sheath has a peak of plasma density near the surface with an excess of slow electrons. In simulations we use the energy dependent secondary emission coefficient, therefore the current of the secondaries increases with the electron beam energy.

In simulations we found that the plate sheath is in a quasi-stable state in the BEE and PEE regimes. Let us consider the evolution of the potential profile during sheath oscillation cycles in our system. Note that in the previous section, the figures showed the plasma parameters averaged over oscillation cycles. We found that the oscillative behavior of the sheath near the floating plate is related to the periodical accumulation of secondary electrons near the plate surface. When the negative charge of secondary electrons achieves some critical value, the plasmoid is transported to the bulk plasma. We found that the sheath oscillates in time with a frequency of about 25 kHz. This frequency is set by the rate of generation of secondary electrons and the ion velocity.

Figure 12(a) illustrates the potential distribution at different times for $j = 10$ mA and $U = -120$ V. A fragment of oscillating floating potential is shown in figure 12(b). The numbers in figure 12(b) point out the time of snapshots of the potential and electron density profiles shown in figures 12(a) and 13. During a cycle of the sheath oscillation near the plate, first, the potential bump forms (curves 1, 2 and 3) and transports the plasmoid of slow electrons to the bulk plasma. In figure 13,

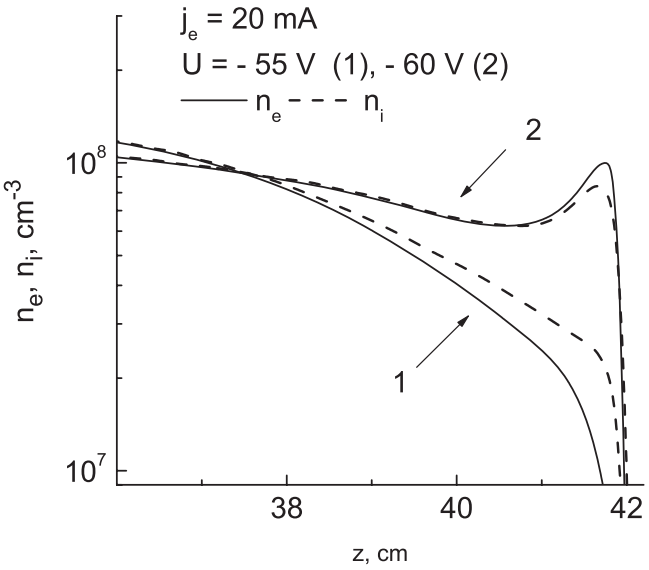

Figure 11. Averaged electron and ion density distributions in front of the plate at $r = 0$, for $U = -55$ V (1, Debye sheath) and -60 V (2, BEE sheath) at $j = 20$ mA. Plate is at $z = 42$ cm.

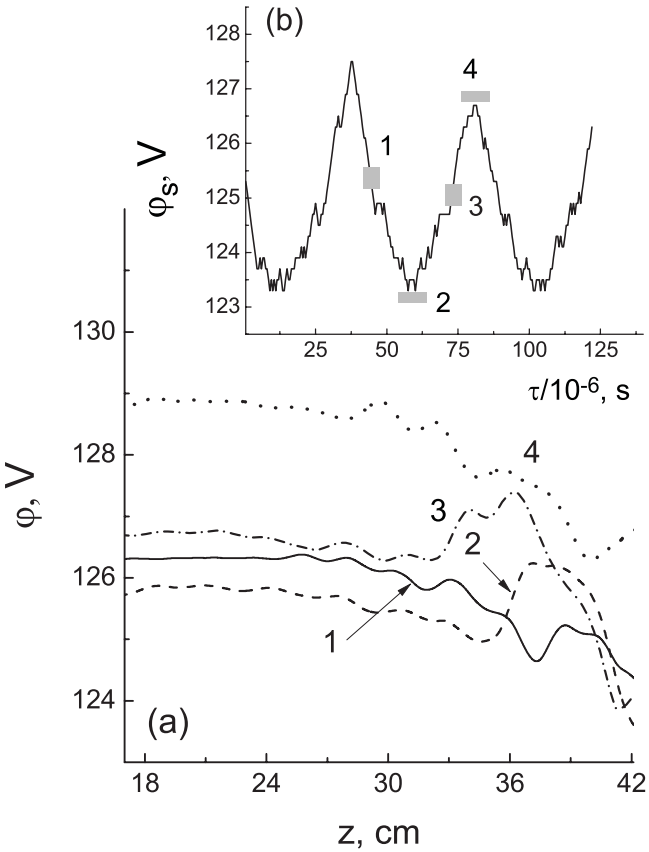

Figure 12. Electrical potential profiles at different time moments (*a*) and fragment of floating plate potential oscillations with time (*b*) for $j = 10$ mA, $U = -120$ V.

the electron density profiles for the same times in the oscillation cycle are shown. The plasmoid starts its motion when the floating potential starts to decrease. The driving potential has a maximum bump when the ϕ_s changes between points 2 and 3 (see figure 12(*b*)). Note that within this time interval, the

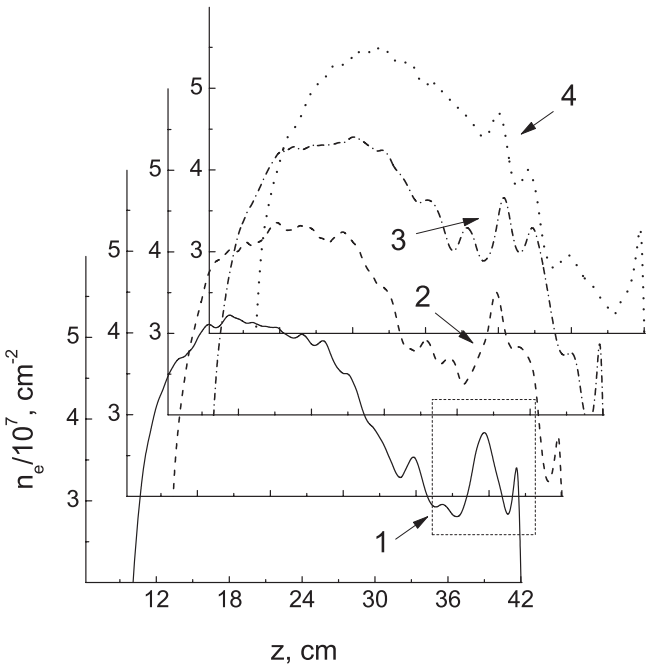

Figure 13. Electron density profiles at different time moments of oscillating floating potential shown in figure 12(*b*) for $j = 10$ mA, $U = -120$ V.

potential bump value is higher than the plasma potential. As soon as the plasmoid moves away from the plate, a new one is accumulated near the surface (see curve 4 in figure 13). The oscillation amplitude of the floating potential of the plate ranges from 2 to 5 V, depending on the negative bias and the thermoemission current.

7. Conclusion

In 2D3V PIC MCC simulations and in the experiment we have studied sheath formation over the emissive floating plate in a dc discharge plasma. The discharge operation in argon at $P = 10^{-4}$ Torr is maintained by the beam electrons emitted from the negatively biased hot cathode. The emissive plate made from Al_2O_3 material has an enhanced electron yield and is placed some distance in front of the hot cathode. We calculated the secondary electron emission by accounting for the energy distribution functions of the electrons approaching the plate surface. Three types of the sheaths have been found near the floating emissive plate and the transition between them was driven by changing the negative bias from -55 to -120 V. First *the Debye sheath* appears near the plate at lower voltages at $|U| < 60$ V, when the secondary electron emission is negligible. With increasing U, the beam electrons bombard the plate with higher energy and the secondary electron emission switches on. It is accompanied by an abrupt potential decrease over the plate sheath and an increase of electron current into the plate by two orders of magnitude. This is a transition between the Debye sheath and a new sheath of *beam electron emission (BEE)* type. For the first time we have found this specific regime of sheath operation near the floating emissive surface. In this regime, the ratio of the potential drop over the plate sheath to the temperature of plasma electrons is $\Delta\phi_s/T_e$

= 4÷5. The floating potential of the plate is controlled by the beam electron current from plasma j_{be} and secondary electron current from the plate j_{es}, $j_{be} + j_{esr} = j_{es}$. The virtual cathode appears and helps to maintain the BEE regime within some voltage range from −60 to −90 V. The virtual cathodeâŁ™ modification changes the backscattering electron current j_{esr}. Further increase of U initiates the smooth transition to *the plasma electron emission (PEE)* sheath regime. In this regime, the ratio $\Delta\phi_s/T_e$ tends to unity with increasing U and the current of plasma electrons to the plate considerably increases. A variation of thermoemission current from the negatively biased cathode from 10 to 40 mA does not affect the qualitative picture of sheath transitions.

In PIC MCC simulations, we have also studied the oscillatory nature of the non-Debye sheath. A plasmoid of slow electrons is formed near the plate and transported to the bulk plasma periodically with a frequency of about 25 kHz.

Acknowledgments

The authors gratefully acknowledge FA9550-11-1-0160 and program manager Mitat Birkan for support of this research. One of the authors, IS, was partly supported by a grant from the Measures to Attract Leading Scientists to Russian Educational Institutions program (contract no. 14.Z50.31.0019).

References

[1] Hobbs G D and Wesson J A 1967 *Plasma Phys.* **9** 85
[2] Sydorenko D, Kaganovich I, Raitses Y and Smolyakov A 2009 *Phys. Rev. Lett.* **103.14** 145004
[3] Campanell M D, Khrabrov A V and Kaganovich I D 2012 *Phys. Rev. Lett.* **108** 255001
[4] Campanell M D, Khrabrov A V and Kaganovich I D 2012 *Phys. Rev. Lett.* **108** 235001
[5] Morozov A I and Savel'ev V V 2007 *Plasma Phys. Rep.* **33** 20
[6] Keidar M, Boyd I D and Beilis I I 2001 *Phys. Plasmas* **8** 5315
[7] Sheehan J P, Hershkowitz N, Kaganovich I D, Wang H, Raitses Y, Barnat E V, Weatherford B R and Sydorenko D 2013 *Phys. Rev. Lett.* **111** 075002
[8] Raitses Y, Smirnov A, Staack D and Fisch N 2006 *Phys. Plasmas* **13** 014502
[9] Intrator T, Cho M H, Wang E Y, Hershkowitz N, Diebold D and DeKock J 1988 *J. Appl. Phys.* **64** 2927
[10] Campanell M D 2013 *Phys. Rev.* E **88** 033103
[11] Sheehan J P and Hershkowitz N 2012 *J. Vac. Sci. Technol.* A **30** 031302
[12] Limpaecher R and MacKenzie K R 1973 *Rev. Sci. Instrum.* **44** 726
[13] Oksuz L and Hershkowitz N 2002 *Phys. Rev. Lett.* **89** 145001
[14] Hershkowitz N, DeKock J R, Coakley P and Cartier S L 1980 *Rev. Sci. Instrum.* **51** 64
[15] Knappmiller S, Robertson S and Sternovsky Z 2006 *Phys. Rev.* E **73** 066402
[16] Hagstrum H D 1954 *Phys. Rev.* **96** 325
[17] Ivanov V V, Popov A M and Rakhimova T V 1995 *Plasma Phys. Rep.* **21** 516
[18] Lagushenko R and Maya J 1984 *J. Appl. Phys.* **55** 3293
[19] Tondu T, Belhaj M and Inguimbert V 2011 *J. Appl. Phys.* **110** 093301
[20] Birdsall C K 1991 *IEEE Trans. Plasma Sci.* **19** 66
[21] Birdsall C K and Langdon A B 1991 *Plasma Physics via Computer Simulations* (Bristol: IOP Publishing)
[22] Babovsky H and Ilner R 1989 *SIAM J. Numer. Anal.* **26** 45
[23] Gimelshein S F, Schweigert V A and Ivanov M S 1999 *Proc. 21st Int. Symp. on Rarefied Gas Dynamics (Marseille, France, 1999)* vol 2, ed R Brun *et al* (Toulouse: Cepadues Editions) 401
[24] Schweigert I V 2012 *J. Exp. Theor. Phys.* **115** 350
[25] Schweigert I V, Kaganovich I D and Demidov V I 2013 *Phys. Plasmas* **20** 101606
[26] Schweigert I V, Ariskin D A, Chernoizyumskaya T V and Smirnov A S 2011 *Plasma Sources Sci. Technol.* **20** 015011
[27] Schweigert I V and Alexandrov A L 2005 *IEEE Trans. Plasma Sci.* **33** 615